Fluctuation Analysis of *Caulobacter crescentus* Adhesion

Elnaz Alipour-Assiabi,* Guanglai Li,* Thomas R. Powers,† and Jay X. Tang*
*Department of Physics and †Division of Engineering, Brown University, Providence, Rhode Island

ABSTRACT The aquatic bacterium *Caulobacter crescentus* divides asymmetrically to a flagellated swarmer cell and a cell with a stalk. At the end of the stalk is an adhesive organelle known as the holdfast, which the stalked cell uses to attach to a solid surface. Often there are two or more cells with their stalks attached to the same holdfast. By analyzing the fluctuations in the stalk angle for a pair of cells attached to a single holdfast, we determine the elastic stiffness of the holdfast. We model the holdfast as three torsional springs in series and find that the effective torsional spring constant for the holdfast is of the order of (10^{-17}–10^{-18}) Nm, with unequal spring constants. The asymmetry suggests the sequence in which the cells attach to each other, and in some cases suggests that strong crosslinks form between the stalks as they make a shared holdfast.

INTRODUCTION

The aquatic bacterium *Caulobacter crescentus* exhibits a dimorphic life cycle (1–6). After an obligatory, free-swimming state known as the swarmer phase, the cell differentiates into a stalked cell by initiating DNA replication, releasing the flagellum and synthesizing a stalk, which is a thin cylindrical extension containing cell-wall and cytoplasm (1). The stalk of a *C. crescentus* cell has a diameter of ~100 nm and a length of up to several micrometers (2,7). Synthesis of the adhesive holdfast occurs early during swarmer cell differentiation, around the time the flagellum is shed. The holdfast appears at the base of the flagellum (8), and later resides at the tip of the stalk, which grows from the same site. The stalked cell elongates as it continues to grow. The stalked cell then synthesizes a flagellum at the pole opposite to the stalked pole, generating an asymmetric cell that divides to produce a new swarmer cell and a stalked cell. Upon division, the stalked cell can immediately begin a new round of DNA replication and cell division, whereas the swarmer cell proceeds with the developmental cycle as described above.

The adhesive holdfast serves to anchor the stalked cells to abiotic and biotic surfaces (1). The aquatic environment of *C. crescentus* cells is often very dilute in nutrients, such as the essential nutrient inorganic phosphate. It has been hypothesized that the ability to remain attached to a surface results in better access to limited nutrients, especially under flow (9). The strength of adhesion depends on the contact between the holdfast and the surface, and the contact between the holdfast and the stalk. A well-known theory for the adhesion of bacterial cells to a solid surface is that the cell is bridged by extracellular polysaccharides (10,11). The *C. crescentus* holdfast is composed of extracellular polysaccharides and additional components such as proteins and uronic acids (9,12). Due to the distinct life cycle, *C. crescentus* provides the simplest model system for study of microbial development and the mechanisms of asymmetric cell division. The ordered synthesis of polar structures, visible by microscopy, allows developmental stages to be easily defined. The synthesis and adhesion of the holdfast play an essential role in the evolution of the stalked cells. Under favorable availability of nutrients, groups of stalked cells are often found to adhere to surfaces via shared holdfasts, forming structures known as rosettes. Although earlier observation found that a group of cells in a large rosette tend to have stalks of the same length (1), it was not shown whether the cells form the attachment simultaneously, or rather build a large rosette while more cells join in and enlarge the shared holdfast. Until now, the precise kinetic steps of rosettes formation have not been well defined.

In a preceding study (13), we have demonstrated an elastic behavior in angular fluctuations of the *C. crescentus* stalked cells, which are attached to a glass surface via their holdfast. We found that the holdfast at the adhesion site provides the elastic coupling that restricts the angular fluctuations. Such an elastic restraint is weakened by orders of magnitude upon additions of lysozyme, an enzyme known to disrupt the network formed by oligomers of N-acetylglucosamine (9). The result shows that the N-acetylglucosamine is largely responsible for the elastic properties of the attachment. In contrast, the stalks behave as rigid rods and contribute negligibly to the angular fluctuation of the attachment. The preceding work also shows evidence of correlated motion of groups of cells sharing holdfasts in small rosettes. However, the previous measurements were not performed with sufficiently high frequency of image recording to determine the correlations quantitatively. In this article, we report on new experiments that record the motion at rates of up to 1000 frames per second of pairs of cells, which attach to the glass surface. We provide a detailed analysis based on a model of coupled springs, which predicts quantitatively the self-correlation of the angular fluctuations of each attached cell as it shares a holdfast with another cell, as well as cross-correlation

Submitted April 15, 2005, and accepted for publication November 28, 2005.
Address reprint requests to Jay X. Tang, Tel.: 401-863-2292; E-mail: jay_tang@brown.edu.

0006-3495/06/03/2206/07 $2.00
doi: 10.1529/biophysj.105.064592

between them. The results from the analysis show frequent occurrence of asymmetry, in the sense that one cell attaches tightly to the glass surface while the second is coupled more tightly to the first cell rather than the glass surface directly. There are also a few clear cases in which the elastic coupling between the two stalks is much stronger than their respective coupling with the glass surface. In all, these results suggest that the two cells likely fuse their holdfast before attachment of the fused holdfast to the glass surface. The results from our analysis shed some light on the precise mechanism of attachment of *C. crescentus* to a substrate.

MATERIALS AND METHODS

C. crescentus strain CB15 wild-type was cultured using peptone-yeast extract medium at 30°C overnight. Then 1 ml of the overnight culture was grown in 10 ml fresh peptone-yeast extract for 4.5 h to mid-exponential phase before preparation of sample slides. A thin glass fiber of a few micrometers in diameter was placed between the coverslip and the glass slide. Rosettes of two or more stalked cells occasionally attached to the glass fiber. All samples were incubated for 3 h at 30°C before observation. After preparing the samples, the rest of the experiment was done at room temperature, ~23°C. A Nikon Eclipse E800 microscope was used for imaging using the phase-contrast mode, with an oil immersion 100× objective lens (Plan Apo; Nikon, Tokyo, Japan).

The fluctuation of the rosette was recorded with a fast camera (Fastcam PCI R2, Photron USA, San Diego, CA) with Photron Fastcam Viewer software. The camera has 512 × 480 resolution, with each pixel covering 74 nm × 74 nm area when used with the 100× objective. Video segments containing 8704 frames were taken at 500 or 1000 frames per second. At such high rates, the image size was reduced to a smaller square of 128 × 120 pixels, which was nevertheless sufficiently large to cover the entire field of interest. Each frame of the fast camera movie was saved as a .jpg file and then imported to MetaMorph (Universal Imaging, Chicago, IL). The center position of the cell body in each frame was determined as described in a preceding publication (13).

The fluctuation angle was calculated as the displacement of the cell from its equilibrium position, divided by the distance between the center of the cell and the position of the holdfast. This distance is noted as r in Fig. 1. The equilibrium position is defined as the position of the cell center averaged over all images. In the actual experiment, there was considerable uncertainty in marking the position of the holdfast where the stalks are attached to the substrate. The round glass fiber to which the cells attach causes significant blurring due to optical diffraction, as the index of refraction of glass does not match that of the water. The error in the holdfast position was estimated to be ~0.5 μm in comparison with the stalk length of 3–5 μm. This was, in fact, a major source of systematic error, which could affect the angles of the two cells differently, depending on their relative orientation with respect to that of the glass fiber.

Another source of possible error is the projection effect, which arises because all angles and distances are measured in their projections onto the plane of focus. In our microscope, the 100× Plan Apo objective lens in combination with the phase contrast feature leads to a depth of focus of ~0.5 μm. Since the cells mainly stayed in focus as they fluctuated, we estimate the angle between the focal plane and the plane formed by the two stalks as $< \sin^{-1}(0.5/4) = 7°$ for a 4-μm-long stalk. We further assume that the out-of-plane fluctuations are comparable to the in-plane fluctuations that we measure. The contribution of the out-of-plane projection to the total deflection is second-order and expected to be much smaller. For example, suppose a stalked cell fluctuates by 5° both out-of-plane and in-plane from its equilibrium position. The in-plane projected displacement perpendicular to the stalk would be ≈0.35 μm, and there would also be a small displacement of 0.02 μm along the stalk due to the out-of-plane motion. Since the projection of the out-of-plane motion is an order-of-magnitude smaller than the in-plane motion, we may safely ignore the out-of-plane motion in this example.

MODEL

Fig. 1 shows the model and an image of the two-cell attachment is shown in Fig. 2. The holdfast with two stalks is represented by three torsional springs. These springs resist changes in the angles θ_1 and θ_2, which describe the angles the rigid stalks make with their respective equilibrium positions. Motion out of the plane of the figure is disregarded, which is justified in the section above.

The elastic energy of the springs is

$$E = \frac{1}{2}\left[k_1\theta_1^2 + k_2\theta_2^2 + k_3(\theta_1 - \theta_2)^2\right] \quad (1)$$

$$= \frac{1}{2}\boldsymbol{\theta}^{\mathrm{T}} K \boldsymbol{\theta}, \quad (2)$$

where $\boldsymbol{\theta}^{\mathrm{T}} = (\theta_1,\theta_2)$, and

$$K = \begin{pmatrix} k_1 + k_3 & -k_3 \\ -k_3 & k_2 + k_3 \end{pmatrix} \quad (3)$$

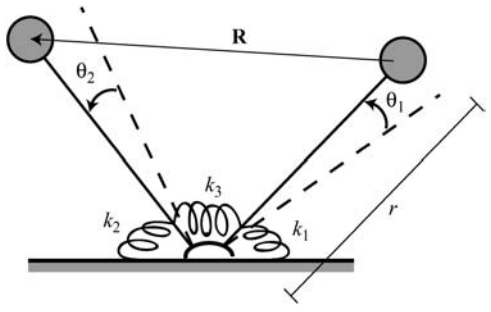

FIGURE 1 A sketch of our model. The θ_i-values are the deviations from the equilibrium position and the k_i-values are the elastic constants of each torsional spring. The counterclockwise direction is positive for all angles.

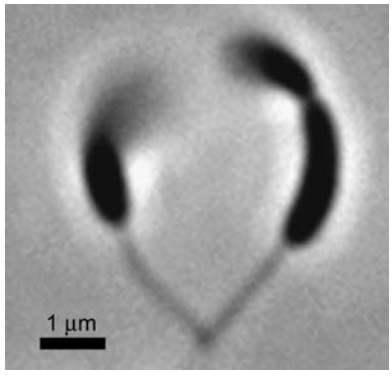

FIGURE 2 A primitive rosette formed by attachment of two stalked cells. The cell on the right is a predivisional cell, indicated by a constriction one-third of the way from the top.

is the matrix of elastic constants, with values determined by the distribution of material in holdfast.

Since the angles θ_1 and θ_2 are small, of the order of 10^{-2} rad, we can use the equipartition theorem and the measured values of $\langle\theta_i(0)\theta_j(0)\rangle$ to determine the elastic constants k_1, k_2, and k_3. By diagonalizing the energy (Eq. 2) and assigning $k_BT/2$ of energy to each mode, we find

$$\langle\theta_i\theta_j\rangle = k_BT(K^{-1})_{ij}, \tag{4}$$

or

$$\langle\theta_1^2\rangle = k_BT\frac{k_2+k_3}{k_1k_2+k_2k_3+k_3k_1}, \tag{5}$$

$$\langle\theta_2^2\rangle = k_BT\frac{k_3+k_1}{k_1k_2+k_2k_3+k_3k_1}, \tag{6}$$

$$\langle\theta_1\theta_2\rangle = k_BT\frac{k_3}{k_1k_2+k_2k_3+k_3k_1}. \tag{7}$$

The angular velocities of the cells are small enough that the Reynolds-number is very low, and the equations of Stokes flow apply to the fluid (14). The linearity of the Stokes equations implies that the velocity $\mathbf{v}_i$ of each cell is a linear function of the forces $\mathbf{f}_i$ on each cell, i.e.,

$$\mathbf{v}_1 = H_{11}\mathbf{f}_1 + H_{12}\mathbf{f}_2, \tag{8}$$

$$\mathbf{v}_2 = H_{21}\mathbf{f}_1 + H_{22}\mathbf{f}_2. \tag{9}$$

If the cells were spheres of radius a separated by a distance $R \gg a$, then to a good approximation, the mobility tensor H_{mn} would be the Oseen tensor (15,16)

$$H_{11}(\mathbf{R}) = H_{22}(\mathbf{R}) = I/\zeta, \tag{10}$$

$$H_{12}(\mathbf{R}) = H_{21}(\mathbf{R}) = 3a(I+\hat{\mathbf{R}}\hat{\mathbf{R}})/(2\zeta|\mathbf{R}|), \tag{11}$$

where $\mathbf{R}$ is the vector connecting the centers of the two spheres (see Fig. 1), $\hat{\mathbf{R}}$ is the direction of $\mathbf{R}$, I is the 3×3 identity matrix, and $\zeta = 6\pi\eta a$ is the drag coefficient for a sphere. Since the fluctuations of the cells about their equilibrium positions are small compared to their separation, we may replace the fluctuating length $|\mathbf{R}|$ in Eqs. 10 and 11 with R, the equilibrium (average) separation between the centers of the two spheres. This simplification eliminates nonlinearities in the dependence on R.

In our situation, the cells are constrained to move along a circle of radius r (see Fig. 1), and we must rewrite Eqs. 8 and 9 in terms of the angles θ_1 and θ_2. Collecting the moments (torques) N_i acting on the cells into the vector $\mathbf{N}$, and assuming the stalks have equal length r, we find

$$\dot{\boldsymbol{\theta}} = M\mathbf{N}, \tag{12}$$

where

$$M = \frac{1}{\zeta r^2}\begin{pmatrix} 1 & 3a/(2R) \\ 3a/(2R) & 1 \end{pmatrix}. \tag{13}$$

The moments arise from a combination of the elasticity of the holdfast and the random Brownian motion of the surrounding fluid, $\mathbf{N} = \mathbf{N}^{el} + \mathbf{N}^{br}$, where $\mathbf{N}^{el} = -K\boldsymbol{\theta}$, and $\mathbf{N}^{br}$ is a random moment with zero mean and white-noise power spectrum. Thus, Eq. 12 amounts to coupled Langevin equations for the angles θ_1 and θ_2,

$$\dot{\boldsymbol{\theta}} = -MK\boldsymbol{\theta} + M\mathbf{N}^{br}. \tag{14}$$

We will use Eqs. 2 and 14 to analyze the data (see also (17)). In the next section, we will show that hydrodynamic interactions are small compared to the effects of the elastic coupling between the two cells. In other words, the main effect of hydrodynamics is to provide a drag resisting the motion of each cell. Therefore, we are justified in making several simplifying approximations in our treatment of hydrodynamic interactions, which are included in the analysis for illustration purposes. The grossest approximation is our use of the off-diagonal terms of Eq. 13, valid for point forces, to represent the hydrodynamic interactions between the two cell-stalk units. Thus, the hydrodynamic interaction will be valid only in order of magnitude. This approximation turns out not to be a severe problem, as we show later that the hydrodynamic interaction plays a much weaker role than elastic coupling. We have also made an implicit assumption that the drag on a cell-stalk unit is concentrated at radius r, with no contribution from the thin stalks. This assumption is inaccurate, since the drag on a thin rod of length r at low-Reynolds-number is comparable to the drag on a sphere with diameter r. A better approximation is to consider the whole cell-stalk unit as a thin rod of length r, and replace ζr^2 in Eq. 13 with the friction coefficient appropriate to the drag averaged over the whole length of the rod, $\zeta_r = \zeta_\perp r^3/3$, where $\zeta_\perp = 4\pi\eta/[\log(2r/d) + 0.84]$ is the resistive-force theory friction coefficient for dragging a rod of length r and diameter d perpendicular to its axis (18).

Based on the argument above, we replace M with $\tilde{M}$ in Eq. 12, where

$$\tilde{M} = \frac{1}{\zeta_r}\begin{pmatrix} 1 & 3a/(2R) \\ 3a/(2R) & 1 \end{pmatrix}. \tag{15}$$

To get expressions for the correlation functions $C_{ij} = \langle\theta_i(t)\theta_j(0)\rangle$, write Eq. 14 in components,

$$\dot{\theta}_i(t) = -(\tilde{M}K)_{ik}\theta_k(t) + \tilde{M}_{ik}N_k^{br}(t), \tag{16}$$

multiply by $\theta_j(0)$, and take the ensemble average. Assuming the average of the Brownian moment $N_k^{br}(t)$ and $\theta_j(0)$ vanish, we find

$$\frac{dC_{ij}}{dt} = -Q_{ik}C_{kj}, \tag{17}$$

where $Q = \tilde{M}K$. The solution to Eq. 17 is

$$C_{ij}(t) = (\exp[-Qt])_{ik}C_{kj}(0), \tag{18}$$

(we assume $t > 0$ from here on), where the equipartition theorem equation (4) determines the constant matrix, $C_{ij}(0) = k_BT(K^{-1})_{ij}$. To evaluate the matrix exponential, we must

diagonalize Q: $Q = P^{-1}\Lambda P$, where Λ is diagonal with elements λ_1 and λ_2, the eigenvalues of Q. Thus,

$$\frac{\langle\theta_i(t)\theta_j(0)\rangle}{k_BT} = \left[P^{-1}\begin{pmatrix} e^{-\lambda_1 t} & \\ & e^{-\lambda_2 t}\end{pmatrix}P\right]_{ik}(K^{-1})_{kj}. \quad (19)$$

In general, Eq. 19 shows that the correlation functions are the sum of two exponentials, e.g.,

$$\langle\theta_1(t)\theta_1(0)\rangle = C_1\exp(-t\lambda_1/\zeta_r) + C_2\exp(-t\lambda_2/\zeta_r), \quad (20)$$

where the different correlation functions have different amplitudes C_i but the same decay constants λ_i/ζ_r. For the case of $k_1 \ll k_2 \simeq k_3$, a common situation in our samples, we find that to the first-order in a/R,

$$\frac{\lambda_1}{\zeta_r} = \frac{k_2}{\zeta_r}\left[\frac{3}{2} + \frac{1}{2}\sqrt{5} - \left(\frac{3}{2} + \frac{3}{4}\sqrt{\frac{2}{5}}\right)\frac{a}{R}\right], \quad (21)$$

$$\frac{\lambda_2}{\zeta_r} = \frac{k_2}{\zeta_r}\left[\frac{3}{2} - \frac{1}{2}\sqrt{5} - \left(\frac{3}{2} - \frac{3}{4}\sqrt{\frac{2}{5}}\right)\frac{a}{R}\right]. \quad (22)$$

The amplitudes C_i has also been calculated analytically, but their form is too lengthy to display here.

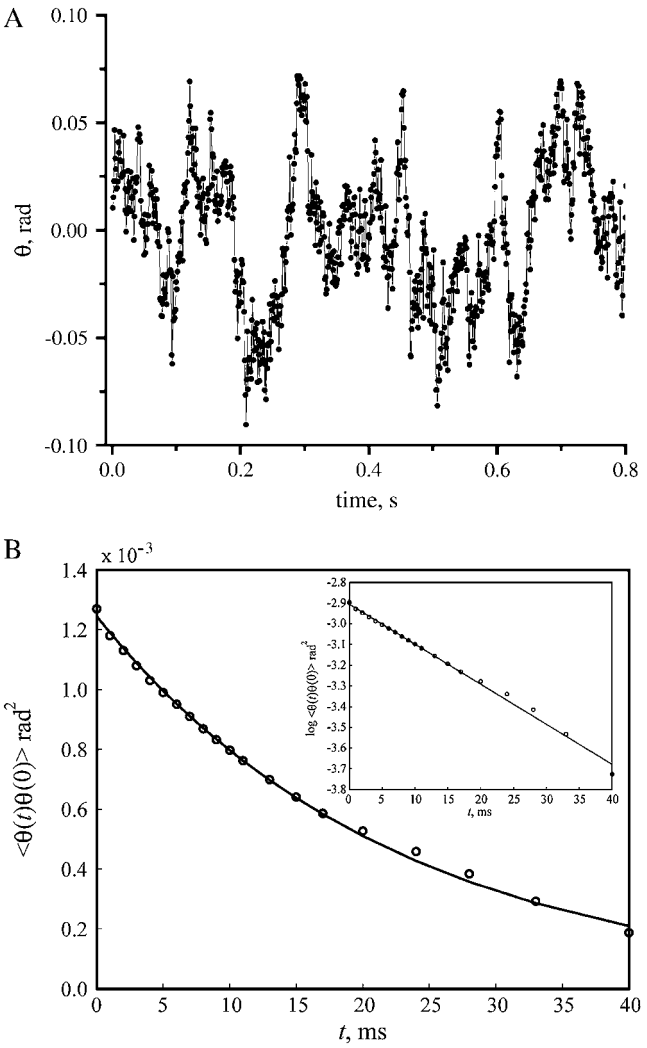

FIGURE 3 (*A*) Raw data of angular fluctuations and (*B*) angular correlation as a function of time for the stalk angle of a single, isolated cell. The solid line is the single exponential fit on the experimental data. Only the points before ($t = 40$ ms) have been used for the fit, since the data become noisy after 40 ms (data not shown).

RESULTS

First, we discuss the measurement of fluctuations of a single, isolated cell. In this case, there is only one stalk connected to the holdfast. We model this situation as a single spring with torsional spring constant k. Fig. 3 *A* shows the fluctuations in the angle θ from the equilibrium value as a function of time and the corresponding correlation function is plotted in Fig. 3 *B*. The value of the correlation time at $t = 0$ is $\langle\theta^2(0)\rangle = 1.27 \times 10^{-3}$ rad^2. Since $\langle\theta^2(0)\rangle = k_BT/k$, we find $k = 3.3 \times 10^{-18}$ Nm for the data in Fig. 3. This value is consistent with the torsional constants measured in Li et al. (13). The time constant of the correlation function is $\tau = 21.5$ ms, which yields $\zeta_r = \tau k = 7.0 \times 10^{-20}$ Nm s. This rotational friction constant corresponds to $r \approx 1.7$ μm, which agrees reasonably well (~50%) with the length of the cell-stalk system (4 μm) measured from the micrograph of the cell (not shown).

We measured the correlation functions $\langle\theta_i(t)\theta_j(0)\rangle$ for eight samples of two-cell rosettes. Using $k_BT = 4.09 \times 10^{-21}$ J and Eqs. 5–7, we calculated the torsional spring constants from the $\langle\theta_i(0)\theta_j(0)\rangle$. The values of the spring constants are reported in Fig. 4 and Table 1. The constants k_1 for samples 1 and 4 are negative. In these cases, the negative spring constant in each sample is almost an order-of-magnitude smaller than the other spring constants in the same sample. Therefore, we interpret the unphysically negative spring constants as being effectively zero. Note that the samples fall naturally into categories, one (samples 6–8) in which k_3 is smaller than both k_1 and k_2, and one (samples 1–5) in which k_3 is comparable to either k_1 or k_2, or sometimes larger than both.

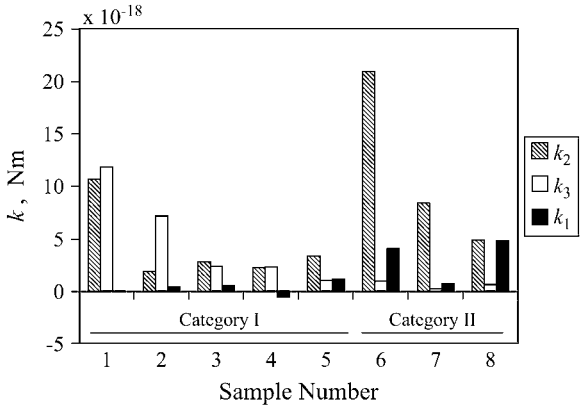

FIGURE 4 A histogram for k_i-values for all the samples studied.

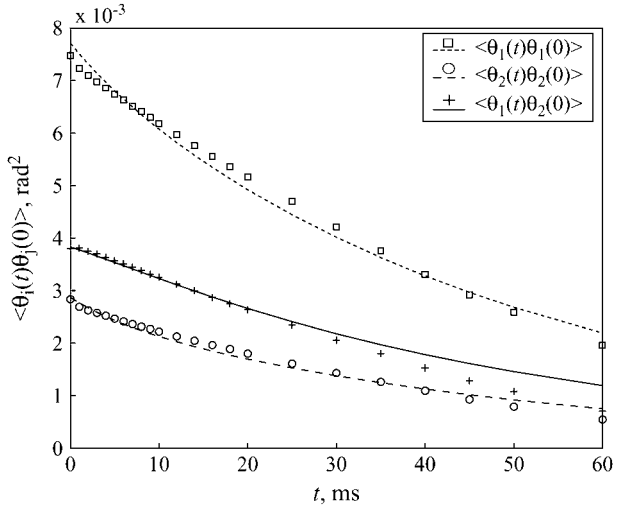

FIGURE 5 Experimental correlation data for sample 4. The curves are fits to the data using our theoretical correlation functions and k_1, k_2, k_3, r_1, and r_2 as fitting parameters.

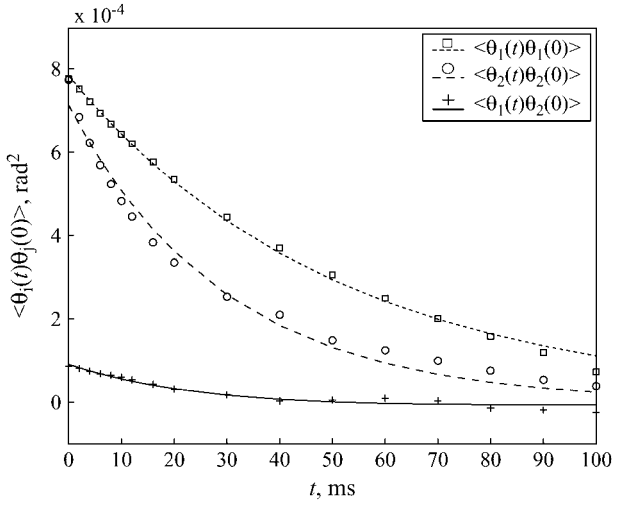

FIGURE 6 Experimental correlation data for sample 8. The curves are fits to the data using our theoretical correlation functions and k_1, k_2, k_3, r_1, and r_2 as fitting parameters.

Figs. 5 and 6 show the measured correlation functions for samples 4 and 8, respectively (see Table 1 for the complete list of samples). These two samples have been chosen as representatives of their respective categories. The curves in these figures have been calculated using our correlation equation (Eq. 19), and fit to the data using k_1, k_2, k_3, r_1, and r_2 as fit parameters. The fits agree well with the data. We get equally good agreement between theory and experiment for five of the remaining six samples (data not shown); sample 1 did not yield comparably good fits. In all cases, the values of r_1 and r_2 from the fits are relatively close to the measured values (see Table 1). The values of the torsional constants from the fits are also generally close to the values calculated from the static measurements (using equipartition as described earlier). Note that these fits also lead to a more reasonable value for k_1 in sample 4.

Table 2 shows the time constants for the correlation functions for all the samples. The discrepancy between $\tau_{1,\mathrm{exp}}$ and $\tau_{1,\mathrm{calc}}$ arises from two sources. These time constants depend on both the torsional spring constants and the drag coefficients. There is a generally small discrepancy between the k_i-values determined from the zero-time correlation function and the fits. There is also a sensitive dependence of the drag coefficient and thus the time constant on the radii r_1 and r_2. To sum up, our model captures the qualitative nature of the correlation functions. Due to the lack of precision in determining the drag coefficients, to get quantitative accuracy, we must fit our theory curves to obtain the parameters.

DISCUSSION

Given our measurements of the torsional stiffness, we can roughly estimate the elastic modulus of the holdfast gel. Dimensional analysis implies $E \sim k/h^3$, where h is the overall size of the holdfast, and k is the typical value of the torsional stiffness. Using $h = 3.4 \times 10^{-8}$ m (see (13)) and $k = 10^{-18}$

TABLE 1 Comparison between measured and fit parameters

		r_1		r_2					K_1		K_2		K_3	
		μm				$\langle\theta_1^2(0)\rangle$	$\langle\theta_2^2(0)\rangle$	$\langle\theta_1(0)\theta_2(0)\rangle$	$\times 10^{-18}$ N m					
Category	Sample	Exp	Calc	Exp	Calc	$\times 10^{-3}$	$\times 10^{-3}$	$\times 10^{-3}$	Exp	Calc	Exp	Calc	Exp	Calc
I	1	2.9	2.9	3.3	3.2	0.754	0.393	0.397	−0.112	−0.0804	10.6	13.6	11.8	11.9
	2	5.1	3.5	5.2	3.6	2.22	1.87	1.77	0.404	0.329	1.84	2.03	7.15	6.73
	3	3.7	2.9	4.1	3.1	2.32	1.29	1.06	0.506	0.645	2.79	2.76	2.36	2.30
	4	3.3	2.6	4.2	2.7	7.47	2.84	3.80	−0.582	0.0530	2.24	2.15	2.31	2.12
	5	3.1	3.1	3.9	3.7	1.14	0.377	0.282	1.13	1.80	10.1	16.3	3.33	5.12
II	6	3.4	3.5	4.1	4.4	0.191	0.843	0.0353	4.04	3.9	20.9	24.5	0.915	1.3
	7	3.6	3.8	2.8	3.5	0.487	4.53	0.110	0.712	0.461	8.35	5.22	0.207	0.674
	8	3.8	3.5	3.0	3.8	0.774	0.776	0.0863	4.80	5.22	4.82	4.68	0.603	0.683

Columns 3–6: Length of the stalks. The heading *exp* refers to stalk length observed in our videos, and the heading *calc* refers to the values of r_1 and r_2 obtained from the fits to theory. Columns 7–9: Equal-time correlations, in rad^2, for eight different samples. Columns 10–15: torsional elastic constants, deduced from the equal-time correlation functions (heading *exp*) and obtained from the fit (heading *calc*).

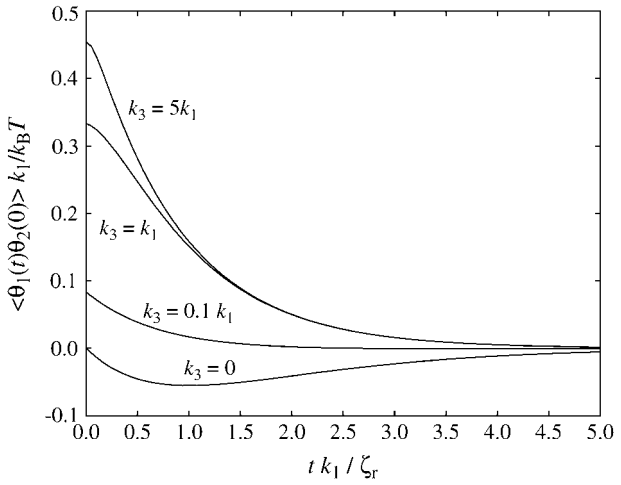

FIGURE 7 Theoretical cross-correlation function versus time for various k_3, for $a/R = 0.1$ and $k_1 = k_2$.

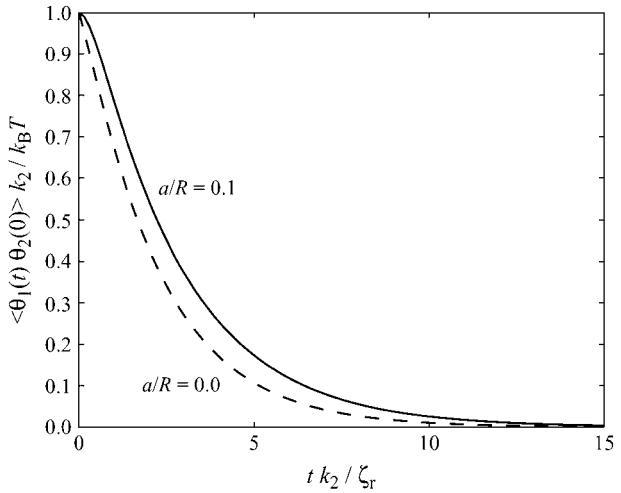

FIGURE 8 Theoretical cross-correlation function versus time for $a/R = 0.0$ and for $a/R = 0.1$ and $k_1 \ll k_2 = k_3$, demonstrating that the hydrodynamic interaction is small.

N m yields $E = 2.5 \times 10^4$ Pa. This value is comparable to that of other biological gels, such as a dense collagen matrix.

For the elastic constants we determined, the elastic coupling between the two cells dominates the hydrodynamic coupling. To illustrate the relative importance of the elastic and hydrodynamic coupling, we consider two special cases. First consider the situation $k_1 = k_2$, such as in sample 8. For this case, the cross-correlation function of Eq. 19 is

$$\frac{\langle\theta_1(t)\theta_2(0)\rangle}{k_BT} = \frac{1}{2k_1}e^{-\lambda_1 t/\zeta_r} - \frac{1}{2k_1 + 4k_3}e^{-\lambda_2 t/\zeta_r}, \qquad (23)$$

where $\lambda_1 = k_1[1 + 3a/(2R)]$ and $\lambda_2 = [k_1 + 2k_3 - (3k_1/2 - 3k_3)a/R]$, to first-order in a/R. When $k_3 = 0$, the coupling is completely hydrodynamic, and we recover the situation of Meiners and Quake (17), in which the cross-correlation function is negative. In the opposite limit, where k_3 is large, the elastic coupling dominates, $\theta_1 = \theta_2$, and the cross-correlation function is positive. The two couplings are comparable when $k_3 \approx k_1 a/R$. Fig. 7 shows the cross-correlation function when $k_1 = k_2$, for various values of k_3. Note the qualitative agreement between the curve with $k_3 = 0.1k_1$ in Fig. 7 and the cross-correlation function of Fig. 6.

The second special case we consider is $k_1 \ll k_2 \simeq k_3$; this case occurs in samples 1–4. For this case, we compare the cross-correlation function with a hydrodynamic interaction and without. Fig. 8 shows that the effect of the hydrodynamic interaction is small when k_3 is comparable to k_1. Fig. 9 shows how the cross-correlation function (with the small effect of the hydrodynamic interaction included) varies with k_1.

TABLE 2 Comparison between measured and calculated time constants

		τ_1		τ_2	
Category	Sample	Exp	Calc	Exp	Calc
I	1	5.34	4.63	22.6	17.1
	2	7.63	15.6	61.2	151.6
	3	10.5	12.6	31.0	37.8
	4	6.11	11.7	49.7	49.6
	5	19.0	26.9	64.6	40.6
II	6	42.1	32.9	69.3	46.1
	7	35.9	32.4	81.4	78.4
	8	29.5	19.2	51.8	70.1

Columns 3–6: Time constants (in milliseconds). In the columns labeled *exp*, the time constant is computed using the k_i-values obtained from the zero-time correlation functions and the drag coefficient calculated from the stalk length measured from the videos. In the columns labeled *calc*, the time constants are obtained from the theoretical correlation functions and values of k_1, k_2, k_3, r_1, and r_2 from the fits.

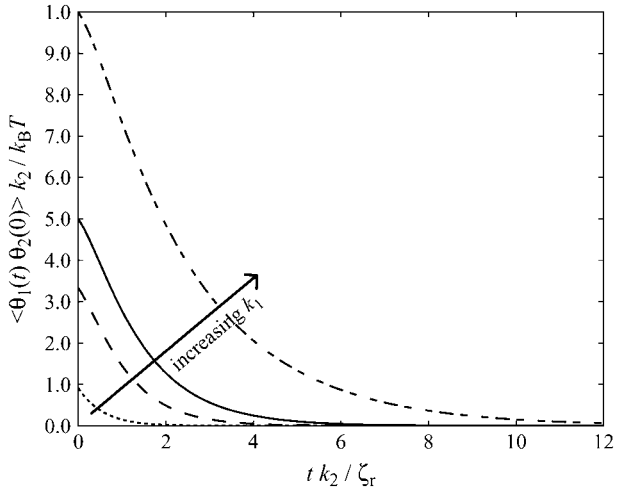

FIGURE 9 Theoretical cross-correlation function versus time for $a/R = 0.1$, $k_2 = k_3$ and varying k_1. (*Dotted line*, $k_1 = 0$; *dashed line*, $k_1 = 0.5\ k_2$; *solid line*, $k_1 = k_2$; and the *dashed-dot line*, $k_1 = 5\ k_2$.)

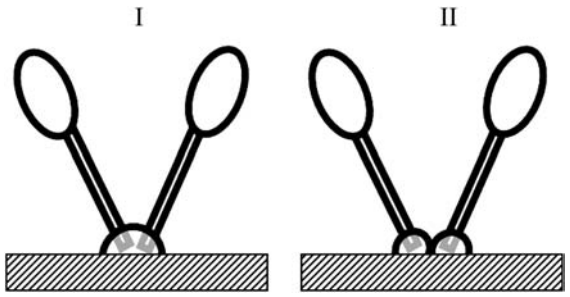

FIGURE 10 Schematic drawings of two possible cell attachments: (*I*) stronger elastic coupling between the stalks; (*II*) weaker elastic coupling between them.

Two possible mechanisms of the rosette formation have been described (1). In the first mechanism, the rosette forms during swarmer stage. In this model, two swarmer cells attach to each other and then the holdfast forms. Therefore, the two cells share a common holdfast in the rosette, which then attaches to the substrate (Fig. 10, *model I*). In this situation, we would expect k_3 to be comparable (or bigger) than k_1 or k_2. The other possibility is that the rosette is formed late in the stalked stage. A stalked cell already has a mature holdfast. The rosette forms when the holdfasts of the two stalked cells collide. However, the two holdfasts are hard to melt into one another, suggesting the situation in Fig. 10, *model II*, which results in a small k_3. Our observations of samples in category I (Table 1) are consistent with *model I* in Fig. 10, and our observations of samples in category II (Table 1) are consistent with *model II* in Fig. 10.

CONCLUDING REMARKS

We have presented throughout this work a method that can be used for measuring mechanical properties of soft gels by observing the Brownian fluctuations of the particles attached to the gel. In this particular system of two cells and a holdfast, we determined the elastic properties of the holdfast, and found that hydrodynamic correlations are negligible. Our observations of the torsional spring constants fall into two categories, one of which is consistent with the collision-fusion model, and the other of which is consistent with the fusion of holdfasts after the cells attach. The validity of these models awaits confirmation by more direct imaging of interaction between cells before their adhesion to substrate. In a separate experiment, we are also measuring the force needed to detach the cell from the holdfast (P. Tsang, G.L. Li, Y.V. Brun, L.B. Feund, and J.X. Tang, unpublished data, 2005). All these studies are aimed at dissecting the mechanical properties of this model microorganism.

We thank Professor Yves Brun for providing the strain CB15, and for a collaborative project leading to this work.

This work was supported in part by National Science Foundation grant No. CMS-0093658 (T.R.P.), NSF grant No. DMR-0405156 (J.X.T.), and NSF grant No. MRSEC DMR 0079964 to Brown University.

REFERENCES

1. Poindexter, J. S. 1964. Biological properties and classification of the *Caulobacter crescentus* group. *Bacteriol. Rev.* 28:231–295.
2. Poindexter, J. S., and G. Cohen-Bazire. 1964. The fine structure of stalked bacteria belonging to the family *Caulobacteraceae*. *J. Cell Biol.* 23:587–607.
3. Poindexter, J. S. 1981. The Caulobacters: ubiquitous unusual bacteria. *Microbiol. Rev.* 45:123–179.
4. Kurtz, H. D., and J. Smith. 1994. The *Caulobacter crescentus* holdfast: identification of holdfast attachment complex genes. *FEMS Microbiol. Lett.* 116:175–182.
5. Brun, Y. V., and R. Janakiraman. 2000. Dimorphic life cycles of *Caulobacter* and stalked bacteria. *In* Prokaryotic Development. Y.V. Brun and L. Shimkets, editors. ASM Press, Washington, DC. 297–317.
6. Ausmees, N., and C. Jacobs-Wagner. 2003. Spatial and temporal control of differentiation and cell cycle progression in *Caulobacter crescentus*. *Annu. Rev. Microbiol.* 57:225–247.
7. Jones, H. C., and J. M. Schmidt. 1973. Ultrastructural study of cross-band occurring in the stalks of *Caulobacter crescentus*. *J. Bacteriol.* 116:466–470.
8. Janakiraman, R. S., and Y. V. Brun. 1999. Cell cycle control of a holdfast attachment gene in *Caulobacter crescentus*. *J. Bacteriol.* 181: 1118–1125.
9. Merker, R. I., and J. Smit. 1988. Characterization of the adhesive holdfast of marine and freshwater Caulobacters. *Appl. Environ. Microbiol.* 54:2078–2085.
10. Robb, I. D. 1984. Stereo-biochemistry and function of polymers. *In* Microbial Adhesion and Aggregation. K.C. Marshall, editor. Spring-Verlag, Berlin. 39–49.
11. Marshall, K. C. 1985. Mechanisms of bacterial adhesion at solid-water interface. *In* Bacterial Adhesion: Mechanism and Physiological Significance. D.C. Savage and M.M. Fletcher, editors. Plenum, New York. 133–161.
12. Umbreit, T. H., and J. L. Pate. 1978. Characterization of the holdfast region of wild-type cells and holdfast mutants of *Asticcacaulis biprosthecum*. *Arch. Microbiol.* 118:157–168.
13. Li, G. L., C. S. Smith, Y. V. Brun, and J. X. Tang. 2005. The elastic properties of the *Caulobacter crescentus* adhesive holdfast are dependent on oligomers of N-acetylglucosamine. *J. Bacteriol.* 187: 257–265.
14. Batchelor, G. K. 1967. An Introduction to Fluid Mechanics. Cambridge University Press, Cambridge.
15. Batchelor, G. K. 1976. Brownian diffusion of particles with hydrodynamic interaction. *J. Fluid Mech.* 74:1–29.
16. Doi, M., and S. F. Edwards. 1986. The Theory of Polymer Dynamics. Oxford University Press, Oxford.
17. Meiners, J.-C., and S. R. Quake. 1999. Direct measurement of hydrodynamic cross-correlations between two particles in an external potential. *Phys. Rev. Lett.* 82:2211–2214.
18. Lighthill, J. 1975. Flagellar hydrodynamics. *SIAM Rev.* 18:161–230.